Food Hydrocolloids 167 (2025) 111424

Contents lists available at ScienceDirect

Food Hydrocolloids

journal homepage: www.elsevier.com/locate/foodhyd

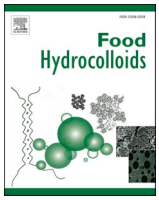

Seed-induced gelation of whey protein via fibril elongation amplification

Rodrigo Sanches Pires [a], Antonio J. Capezza [b], Mathias Johansson [c,1], Maud Langton [c], Christofer Lendel [a,*]

[a] Department of Chemistry, KTH Royal Institute of Technology, Teknikringen 30, SE-100 44, Stockholm, Sweden
[b] Department of Fibre and Polymer Technology, KTH Royal Institute of Technology, Teknikringen 56-58, SE-100 44, Stockholm, Sweden
[c] Department of Molecular Sciences, Swedish University of Agricultural Sciences, BioCentrum, Almas allé 5, SE-756 61, Uppsala, Sweden

ARTICLE INFO

Keywords:
Protein nanofibrils
Hydrogel
Sol-gel transition
Percolation
Seeding
Whey protein

ABSTRACT

Protein nanofibrils (PNFs), especially those from the whey protein β-lactoglobulin, hold the promise for applications in food technology, medicine, and sustainable materials. In this work, we explore the mechanisms underlying the sol-gel transition of whey protein isolate triggered by pre-fragmented whey fibrils (seeds) at low pH and high temperature. We show that, under these conditions, the formed hydrogels are constructed from PNFs. The presented results suggest that the seeds amplify the fibril growth process by providing active ends that capture peptide monomers produced via acid hydrolysis. This changes the fibrils' length distribution (up to 10-fold increase of their average contour length), and the samples reach the percolation threshold at a much lower mass concentration of fibrils. We also note that seeding has a strong impact on morphology and catalyzes a conversion of short, curved fibrils into long straight ones, which also contribute to the lower percolation limit. Rheological measurements indicate that attractive inter-fibrillar forces stabilize the PNF network. This is further evidenced by the gels' resistance to disassembly across a wide pH range, implying that other forces than electrostatics are important for stabilizing the fibrillar network. Finally, we discuss the nature of the sol-gel transition based on continuum percolation theory, which corroborates the observed relationship between PNF length distribution and the sol-gel transition.

1. Introduction

Many polymeric systems can self-assemble to form networks and gels through various mechanisms. Assembled three-dimensional networks in the form of hydrogels are important for a range of food applications (Cao & Mezzenga, 2020). One frequently studied proteinaceous system that can readily form hydrogels is β-lactoglobulin, an 18.4 kDa highly hydrophilic whey protein (Uniacke-Lowe & Fox, 2022). Upon heating, the globular structure of β-lactoglobulin partially unfolds, promoting self-assembly in the form of colloidal aggregates whose properties and shapes are pH- and ionic strength-dependent (Langton & Hermansson, 1992; Puyol et al., 2001; Stading & Hermansson, 1990, 1991). At pH values far from the isoelectric point and low ionic strength, strand-like aggregates form upon heating (Gosal et al., 2004; Kavanagh et al., 2000; Langton & Hermansson, 1992; Veerman et al., 2002). These strand-like aggregates, known as amyloid-like protein nanofibrils (PNFs), can be regarded as a class of one-dimensional nanomaterials of proteinaceous origin. The very high surface area, intrinsic rigidity, and the fact that PNFs possess the properties of chirality and polarity along their main axis make them very attractive building-blocks for materials (Knowles et al., 2007; Lendel & Solin, 2021; Roode et al., 2019). Despite the historical association of amyloid nanofibrils with disease, recent evidence demonstrated the biosafety of food protein-derived PNFs, which opens for applications in materials, food and biomedical products (Rahman et al., 2023; Xu et al., 2023).

Several protocols have been employed to produce fibrils with different properties from β-lactoglobulin (Hoppenreijs et al., 2022; Loveday et al., 2017). The most common of these methods, heating the protein solution under acidic conditions, leads to partial hydrolysis of the protein and PNFs form via self-assembly of aggregation-prone peptides (Akkermans et al., 2008; Ye et al., 2018). PNFs can also be produced from whey protein isolate (WPI), an industrial side stream from

This article is part of a special issue entitled: Boosting structural food science published in Food Hydrocolloids.

* Corresponding author.
E-mail address: lendel@kth.se (C. Lendel).
[1] Present address: Department of Chemistry and Chemical Engineering, Chalmers University of Technology, Kemigården 4, SE-412 96 Gothenburg, Sweden.

https://doi.org/10.1016/j.foodhyd.2025.111424
Received 17 July 2024; Received in revised form 25 March 2025; Accepted 6 April 2025
Available online 7 April 2025

the dairy industry, and these fibrils are reported to exclusively consist of β-lactoglobulin-derived peptides (Akkermans et al., 2008; Bateman, Ye, & Singh, 2010; Bolder et al., 2006; Dave et al., 2013).

PNFs can be classified as flexible, semi-flexible or stiff spherocylinders based on the relation between the contour length and the persistence length (Hoppenreijs et al., 2022) and the morphology of the formed PNFs can be controlled by various extrinsic factors such as pH and ionic strength (Hoppenreijs et al., 2022). For β-lactoglobulin (and WPI), there is an obvious morphological shift between flexible (also described as 'curved', 'curly' or 'worm-like') and semi-flexible/stiff ('straight') PNFs controlled by the initial protein concentration, with high concentrations resulting in flexible fibrils and low concentrations in the fibrils that are straight (vandenAkker, Engel, Velikov, Bonn, & Koenderink, 2011; Ye et al., 2018). The explanation for this behavior may be related to the lengths and amino acid sequences of the peptide building blocks resulting from hydrolysis (Housmans et al., 2022; Ye et al., 2018).

In previous work (Ye et al., 2018), we noticed a peculiar behaviour demonstrated by WPI when fibrillated in the presence of *seeds,* i.e. short fragmented PNFs obtained via either sonication or freeze-thawing (Chiti & Dobson, 2006; Jarrett & Lansbury, 1993; O'Nuallain et al., 2004). The addition of seeds to the WPI solution eventually resulted in a sol-gel transition into self-standing gels, a feature only observed at very high (>90 g/L) concentrations of unseeded WPI. The formation of fibrillar gels from β-lactoglobulin is well-established (Gosal et al., 2004; Kavanagh et al., 2000; Langton & Hermansson, 1992; Veerman et al., 2002) and percolation theory gives that, for high aspect-ratio rod-shaped particles, such as PNFs, the percolation limit should be at very low fibrillar volume fractions (Boissonade et al., 1983; Kyrylyuk & van der Schoot, 2008; Otten & van der Schoot, 2009; Philipse, 1996; Philipse & Verberkmoes, 1997; Schilling et al., 2015; Wouterse et al., 2009). However, the soft electrostatic repulsion between PNFs at low pH contributes to the stabilization of a colloidal suspension and prevents gelation.

Seeds can indeed have significant effects on fibrillation kinetics. When added to a solution with aggregation-prone monomers, seeds help bypass the high energy barrier associated with fibril nucleation. The seeds provide ends onto which new monomers can attach and elongate the fibrils (Arosio et al., 2015; Buell, 2019; Scheidt et al., 2019). Moreover, the seeds can also provide active surfaces onto which new monomers can attach and form new nuclei, a process referred to as secondary nucleation (Cohen et al., 2013; Linse, 2017; Scheidt et al., 2019; Thacker et al., 2023; Törnquist et al., 2018). Considering the combined effect of these processes, it is obvious that fibril formation will be faster in the presence of seeds, but not how the seeds could determine if a gel is formed or not. A recent study reported seed-mediated gelation of lentil proteins (Shi & Dee, 2024). However, the mechanistic details underlying the sol-gel transition and the effects of the seeds on this process were not discussed in that work.

The study presented here aims to understand and explain the mechanistic nature behind the sol-gel transition observed in seeded WPI solutions. We first explore the phase diagram to determine which parameters control the gelation. Then, we move on to analyze the fibrillation process in seeded and unseeded samples in terms of assembly kinetics, fibril yield and PNF morphology. Finally, we examine the structural and mechanical properties of the formed gels to elucidate the nature of the inter-fibrillar forces.

2. Materials and methods

2.1. WPI preparation

WPI powder (Lacprodan DI-9224, Arla Food Ingredients, Denmark) was dissolved in 0.1 M HCl (aqueous solution) to a concentration above 100 g/L and stirred at room temperature until fully solubilized. The resulting aqueous solution was then dialyzed with a 6–8 kDa molecular weight cut-off membrane (Spectrum laboratories, Rancho Dominguez, CA, USA) to remove impurities and shorter protein fragments. Dialysis was performed against 0.01 M HCl (aqueous solution, pH 2) under constant stirring for 24 h at room temperature. The protein concentration of the resulting dialyzed WPI solution was measured using dry-weight and stored at 4 °C until further use.

2.2. Seed preparation

The fabrication of seeds follows previously used protocols (Ye et al., 2018). Briefly, dialyzed WPI solution was diluted with 0.01 M HCl (aqueous solution, pH 2) to 35 g/L and incubated at 90 °C for 2 days to promote fibrillation and the formation of long and straight (semi-flexible) PNFs. The resulting PNF solution was then further dialyzed with a 100 kDa cut-off membrane (Spectrum laboratories, Rancho Dominguez, CA, USA) against 0.01 M HCl (aqueous solution) for 2 days to remove non-fibrillar material. Freeze-thawing was then employed to generate fragments (seeds) with shorter contour lengths than their mature-fibril counterparts. First, the purified PNFs formed at pH 2 were frozen at −20 °C for 24 h and then thawed by submerging the frozen solution in a water bath at 25 °C. A total of three similar freeze-thawing cycles were performed to generate the seeds.

2.3. Gelation, hydrolysis and fluorescence intensity

For gel formation, we prepared WPI solutions in an identical manner to that of WPI seed preparation, but at three different pH conditions (pH = 1.5, 2.0 and 2.5) and various WPI (10, 20, 40 and 60 g/L) and seed (0, 1, 2.5, 5, 10 wt% of WPI) concentrations added pre-incubation. All aliquots were vortexed to ensure proper mixing and then incubated at 90 °C. Gelation was performed either in 15 mL plastic tubes (5 mL per sample and 3 replicates) or, for rheological measurements, in 48 mL glass bottles (10 mL per sample and 5 replicates) (Wheaton, Millville, NJ, USA). To build the phase diagram for each sample condition, and to record the time for sol-gel transition, we inverted the tubes with the aliquots and observed sample behavior. Fully formed gels were the ones in which there was no sample flowing down the walls of the tubes (Fig. 1G). Samples where only a portion of the total volume had experienced gelation were considered "locally gelled" (Fig. 1G). For the phase diagram, the solutions were incubated for a total of 32 h. After incubation, the samples were transferred to a fridge (4 °C) for 20 min to stop aggregation. Following this step, the samples were placed on the lab bench for 2 h to reach ambient temperature (ca. 23 °C) and their pH were measured using a benchtop pH meter (Seven Compact S220, Mettler Toledo) and an Ultra-Micro-ISM electrode (Mettler Toledo). The pH measurements were also performed prior to incubation to detect the pH variation in each sample after incubation. The gelled samples were diluted by adding 7 mL of 0.03 M HCl (aqueous solution, pH 1.5) to each of the 5 mL samples and vortexed until proper mixing and gel dissolution were achieved. In the cases where gel formation had occurred, mixing was performed until no visible gel clumps were observed. The samples corresponding to the different time points were then mixed with an aqueous Thioflavin T (ThT) solution (Sigma Aldrich) to a final concentration of 20 μM ThT. The dye thioflavin T is commonly used to detect amyloid formation in protein mixtures due to its pronounced increase in fluorescence intensity upon binding to the protein (Gade Malmos et al., 2017). Samples were then transferred to a 96 well-plate (Corning 3881, Corning, NY, USA) and the fluorescence was measured with a FluoStar plate reader (BMG biotech, Germany) using bottom optics and excitation at 440 nm and emission at 482 nm.

2.4. Fibrillation kinetics

Fibrillation was studied in an off-line manner. Eight different sample conditions (10, 20, 40 and 60 g/L with/without seeds) were studied at pH 1.5 and 90 °C, with 3 replicates for each time point. To ensure

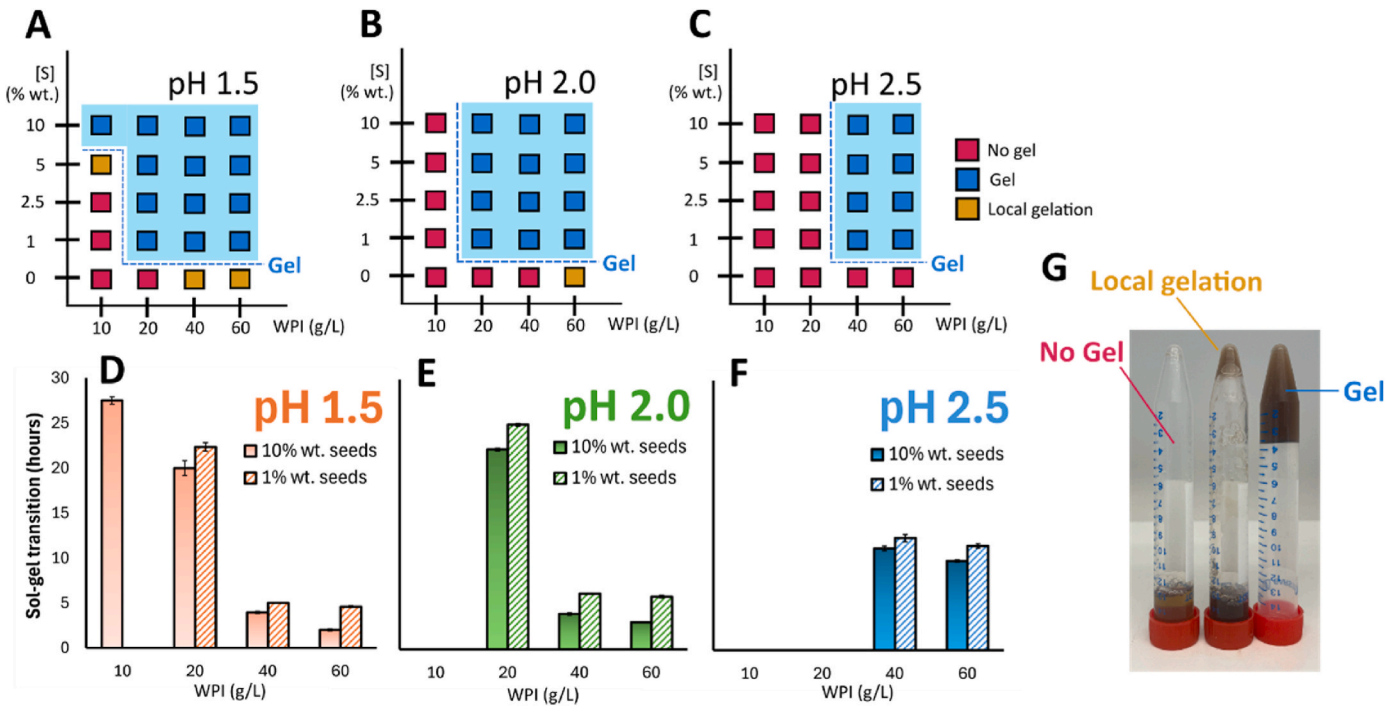

Fig. 1. (**A-C**) Phase diagram for seed-induced gelation of WPI as a function of pH, seed concentration [S], and WPI concentration after 32 h incubation at 90 °C. (**D–F**) Sol-gel transition times using the inverted tube method of the samples with 1 % and 10 % seeds and different pH. (**G**) Photograph exemplifying the phase-transition criteria applied to build panels **A** to **F**. The brown colour of the samples is likely a product of the presence of residual sugars in WPI. (For interpretation of the references to color in this figure legend, the reader is referred to the Web version of this article.)

reproducibility, we prepared large volumes of stock solutions for each fibrillation condition and aliquoted the volume into 15 mL plastic tubes. A total volume of 5 mL per tube was used, with a total of 3 replicates for each sample (similar procedure as described in 2.4). All the tubes were then incubated at the designated temperature and removed at different times. ThT fluorescence measurements were done with sample preparation, dilution and measurement performed in the same manner as already described (section 2.4). The replicates for each time point were averaged, and a simple adaptation of a sigmoidal model (Gade Malmos et al., 2017) was used to fit the ThT fluorescence data (Y) as a function of time (t):

$$Y(t) = Y_i + \frac{Y_f - Y_i}{1 + e^{((t-t_{1/2})/\tau)}} \quad (1)$$

Where Y_i is the initial ThT fluorescence intensity, Y_f is the intensity at plateau ThT value, $t_{1/2}$ is the half-time of the reaction (representing the time needed to reach halfway through the elongation phase) and τ the elongation time constant.

2.5. Atomic force microscopy

To image fibril morphology, each hydrogel sample was diluted between 50 and 5000 times in a 0.01 M HCl (aqueous solution). Immediately after dilution, 25 μL of each sample was deposited onto freshly cleaved mica and incubated for 10 min at room temperature. Following the incubation step, samples were washed using filter-sterilized Milli-Q water and dried using a stream of compressed air. Fibrils were imaged using an ICON Dimension AFM (Bruker) with NanoScope Software (version 8.1, Bruker) controller operating ScanAsyst in air mode and using ScanAsyst-AIR-HPI probes (Bruker, tip radius 2 nm, spring constant: 0.25 N/m, frequency: 55 kHz). To ensure proper high-resolution imaging, extra care was taken to minimize any deformation of the fibrils by the probe itself. To achieve this, tapping parameters were manually set to ensure the lowest driving amplitude and amplitude setpoint possible, while still being enough to get a proper topology signal. Nanoscope analysis software (Version 1.9, Bruker) was used to process the image data by flattening the height topology data and removing the tilt and scanner bow. Further statistical analysis of the sample contents was carried out using the fiber tracking software FiberApp (Usov & Mezzenga, 2015).

2.6. Fibril yield by dialysis

To study fibril yield at sol-gel transition time, samples with WPI (10, 20, 40 and 60 g/L) and seeds (between 0 and 10 % wt. WPI) were prepared, removed from incubation (90 °C) once a gel was formed and diluted exactly as described in section 2.4. After the dilution step, 5 mL (V_i) of each sample were transferred into a small 100 kDa dialysis membrane (Spectrum laboratories, Rancho Dominguez, CA, USA) and sealed with clamps. The membranes were sealed with little to no air. Each dialysis membrane with the sample was then immersed in 100 mL ($V_{dialysate}$) 0.03 M HCl in individual glass beakers for 36 h. After this time interval, the dialysates (with only unfibrillated material) were measured for dry weight and their concentrations ($[U]_{out}$) were recorded. The concentration of unfibrillated material inside the membrane $[U]_{in}$ is $[U]_{out} = [U]_{in}$ and the total mass of unfibrillated material $M_{U,total} = [U]_{out} \times V_{dialysate} + [U]_{out} \times V_i$. The initial concentration of fibrillated material $[F]$ in each sample was then recorded as follows:

$$[F] = [P]_i - \frac{[U]_{out} \times (V_{dialysate} + V_i)}{V_{initial}} \times df \quad (2)$$

Where $[P]_i$ is the initial concentration of WPI and df is the dilution factor prior used to prepare the samples prior to dialysis.

2.7. Critical point drying

Gels were carefully removed from their 15 mL plastic tubes and immersed in a bath of ethanol. This aqueous solution started at 10 %

ethanol, and its content was slowly incremented by changing the solution every day in steps of 10 % until 100 % was reached. A highly transparent gel was obtained. The solvent-exchanged gels were then dried for 4 h using an Autosamdri-815 Series A critical point drying (Tousimis, US). The dried gels were stored in a desiccator until further use.

2.8. Scanning electron microscopy

A field-emission scanning electron microscope (FE-SEM, Hitachi S4800, Japan) was used for the microstructural analysis (1–3 kV accelerating voltage). The dried materials were immersed in liquid nitrogen and cryo-fractured inside the liquid nitrogen to ensure a cryogenic fracture. The fragments of the foams were placed carefully on carbon tape and sputtered using a gold target for 3 min.

2.9. Oscillation rheology

For rheological measurements, 10 mL seeded WPI gels were prepared by incubation for 24 h at 90 °C and pH 1.5 in 48 mL glass bottles (Wheaton, Millville, NJ, USA). A DHR-3 rheometer (TA Instruments, New Castle, DE, USA) equipped with 20 mm stainless steel plate geometry was used. Due to the soft nature of the gels and to reduce artefacts in our measurements, we performed all rheological measurements with the gels inside the glass bottles. Since the diameter of the plate geometry was smaller than that of the glass vials (diameter of 53 mm), the measured rheological values are overestimated. The glass bottles were fixed onto the bottom plate using terracotta. Frequency sweeps were performed at 0.1 % strain between 0.1 and 100 Hz. As the height of the individual hydrogels in the glass vials varied slightly, different gaps were used to perform the measurements (2960–3240 μm). The applied strain value was based on preliminary experiments and the determination of linear viscoelastic region given the sample and experiment conditions. After the frequency sweep, an oscillation sweep was performed in the same sample between 0.01 and 100 % with an angular frequency of 10 rad/s. All experiments were performed at room temperature and 5 replicates were measured in total.

3. Results and discussion

3.1. Sol-gel transition of seeded WPI

We first studied how gel formation is affected by seed concentration (between 1 % and 10 % seed mass compared to WPI mass), WPI concentrations (10–60 g/L) and pH (1.5–2.5) to establish a phase diagram for the process. The final states of the samples after 32 h of incubation are summarized in Fig. 1A–C. The choice of the incubation period of 32 h was to ensure that the sol-gel transition would be observed for all WPI solutions capable of forming a gel, even those that might experience very slow gelation. At the lowest pH, gelation occurs at low WPI concentrations (20 g/L) and even at 10 g/L with the higher seed concentration. A similar phase behavior can be seen for the samples incubated at pH 2, except for the 10 g/L sample, which, in this case, does not gel even at the highest seed concentration. The role of pH in gel formation can be further emphasized by the fact that at pH 2.5, the sol-gel transition with seeds only occurs at WPI concentrations equal to and above 40 g/L. A few additional differences can be seen between the samples regarding what we define as "local gelation" (see Fig. 1G). For instance, we see that unseeded WPI at 40 and 60 g/L (pH 1.5) forms some gel clumps, an observation that extends only to the 60 g/L samples when incubated at pH 2. Taken together, only samples to which seeds have been added form *stable* gels, as assessed using the inverted tube method (Fig. 1G), under the investigated conditions.

The observed sol-gel transition times with 1 % or 10 % added seeds (determined by sample inversion) at the investigated conditions are presented in Fig. 1D–F. Interestingly, the higher seed concentration seems to only slightly promote a faster sol-gel transition, regardless of the pH and initial WPI concentration used. Hence, we can conclusively say the presence of seeds is an explicit requirement for the sol-gel transition of WPI solutions to occur under these conditions. However, the amount of seeds only slightly influences the kinetics of gel formation. Instead, gelation time is mainly defined by the initial WPI concentration and pH (Fig. 1A–F), with higher WPI concentration and lower pH promoting faster gelation.

3.2. WPI forms nanofibrils under the applied incubation conditions

Investigations of the gel samples by AFM revealed the presence of nanofibrils under all conditions (Fig. S1). This is in agreement with previous studies that link gelation with the formation of PNFs (Gosal et al., 2004; Kavanagh et al., 2000; Langton & Hermansson, 1992; Veerman et al., 2002). As outlined in the introduction, seeding can significantly affect the fibrillation process and thereby provide an obvious link between the self-assembly of WPI into PNFs and the sol-gel transition. However, fibril formation *per se* does not explain the selective gelation of seeded samples since fibrils are present in all samples incubated at low pH and high temperature (see Fig. S1).

3.3. Faster hydrolysis results in the formation of more fibrils

The strong dependence of the gelation on WPI- and H^+ (pH) concentrations (Fig. 1) suggests that protein hydrolysis may have a central role in the sol-gel transition. This is in line with previous work, suggesting that acid-based proteolysis is the rate-limiting step in WPI fibrillation (Ye et al., 2018). At lower pH (thus higher H^+ concentration), a higher rate of hydrolysis is expected, which should translate into the formation of a higher number of peptide-building blocks for fibril formation (Akkermans et al., 2008; Ye et al., 2018), thus leading to higher PNF content. A simple yet effective method to follow hydrolysis is by monitoring pH changes, as each peptide bond cleavage consumes one H^+ ion. We used this method to investigate the relationship between WPI- and H^+ concentrations and we observed larger pH variations with decreasing initial pH and increasing WPI concentrations (Fig. 2A and B). This is expected because a higher number of available peptide bonds (due to increased WPI concentration) combined with a greater number of free hydrogen ions leads to a higher turnover of hydrolyzed bonds. Importantly, the presence of seeds did not affect the degree of hydrolysis under identical pH conditions (Fig. 2A and B).

In addition, we investigated the amount of fibrillar material formed during the incubation by the means of ThT fluorescence. A clear increase in ThT fluorescence with decreasing pH is evident for all WPI concentrations when seeds are present, but no such increase is observed in the absence of seeds (Fig. 2C). Interestingly, seeded samples (which form gels) consistently exhibited higher ThT fluorescence across all pH conditions than their unseeded counterparts (Fig. 2C). Although ThT fluorescence intensity is not strictly quantitative, the increased signal strongly suggests a greater fibrillar mass when seeds are added, linking gelation to the presence of more fibrillar material.

Based on these observations we hypothesize that the seeds amplify fibril formation by "capturing" the peptide-building blocks formed when WPI is randomly hydrolyzed. The idea of faster recruitment of the formed monomers into the aggregation pathway is especially relevant in the context of the fibrillation of proteins under hydrolysis-promoting conditions since newly formed PNF-compatible peptides can still undergo further degradation. This model also explains the minor effect of seed concentration in sol-gel transition time since the seed concentration only needs to be enough to capture all new peptides. Higher concentrations of seeds will, therefore, not change the rate of fibril build-up. Similar results were reported for seeding the fibril formation of lentil proteins (Shi & Dee, 2024). Notably, the number of *seed ends* available for elongation does not change by adding monomers to the ends. Hence, if the number of ends is larger than the production of new

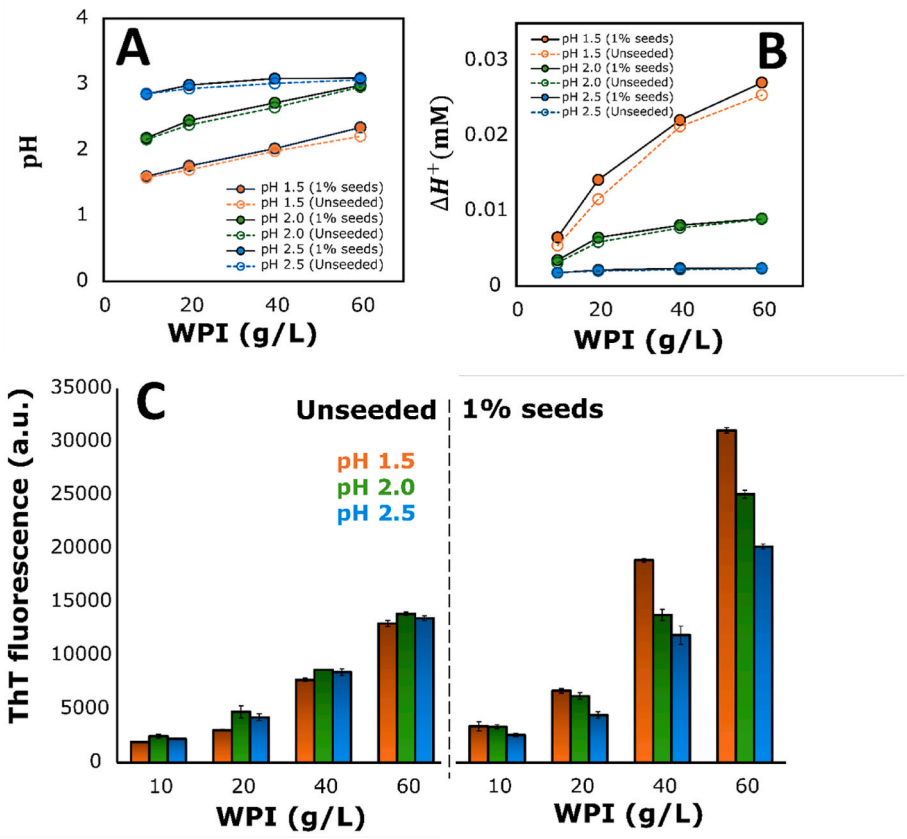

Fig. 2. Correlation between pH and WPI concentration (**A**) and between the change in H^+ concentration (ΔH^+) and WPI concentration (**B**) in the presence and absence of seeds after 32 h incubation. (**C**) ThT fluorescence intensities of unseeded and seeded samples after 32 h incubation.

elongation-capable monomers, the seed concentration will only have minor effects on the fibril elongation rate.

3.4. Seed effect on the fibrillation rate

The results presented so far provide some insights into the relationship between fibrillation and gel formation, but they do not explain why only the seeded samples undergo a sol-gel transition since PNFs are present in all samples. To further elucidate a link between the rate of fibril formation and gelation, we investigated PNF assembly kinetics by following the ThT fluorescence over time (Gade Malmos et al., 2017). As the lowest pH (pH 1.5) and highest seed concentration (10 % wt. WPI) conditions promote gel formation across all studied WPI concentrations, we decided to focus on these samples. The ThT kinetics results for seeded and unseeded samples are displayed in Fig. 3A and B, respectively. The first point to be made is that the addition of seeds results in a very small increase in ThT fluorescence at the starting time but a pronounced difference in plateau values. This is a direct indication that the fibril mass at the sol-gel transition is higher than that introduced into the system by the seeds. We further examined the presented assembly kinetics of the

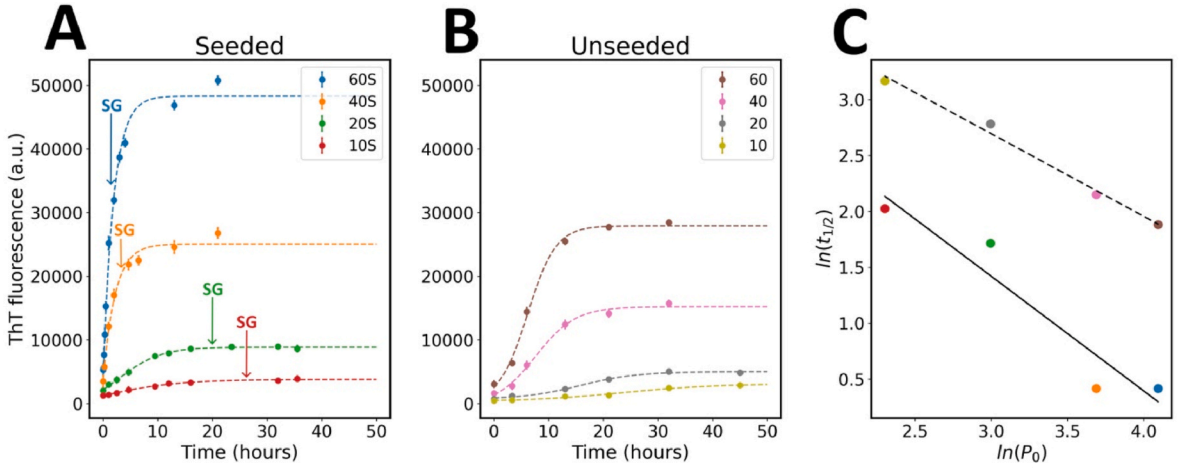

Fig. 3. (**A, B**) ThT fluorescence kinetics of seeded (**A**) and unseeded (**B**) WPI. The values 10, 20, 40 and 60 represent the initial WPI concentration (g/L) and the letter "S" designates samples with seeds. The lines represent the sigmoidal fits and the sol-gel transition times (taken from Fig. 1D) are indicated as "SG" and arrows. (**C**) Double-logarithmic plot of the half-times extracted from the fitted ThT curves in panels A and B versus the initial WPI concentration (P_0).

PNFs by fitting the ThT data to a simple sigmoidal model (see methods section) (Gade Malmos et al., 2017). As fibrillation of β-lactoglobulin proceeds via acid-induced hydrolysis and is dependent on the rate of formation of peptide building blocks (Ye et al., 2018), fitting of the kinetic data to models describing the aggregation in terms of rate constants for microscopic processes (Meisl et al., 2016) to derive the underlying molecular mechanisms is not possible without extensive modification of the models. The kinetic data show that the PNF formation is faster at higher WPI concentrations, both in the presence and absence of seeds (Fig. 3A and B). There is also a clear acceleration of the

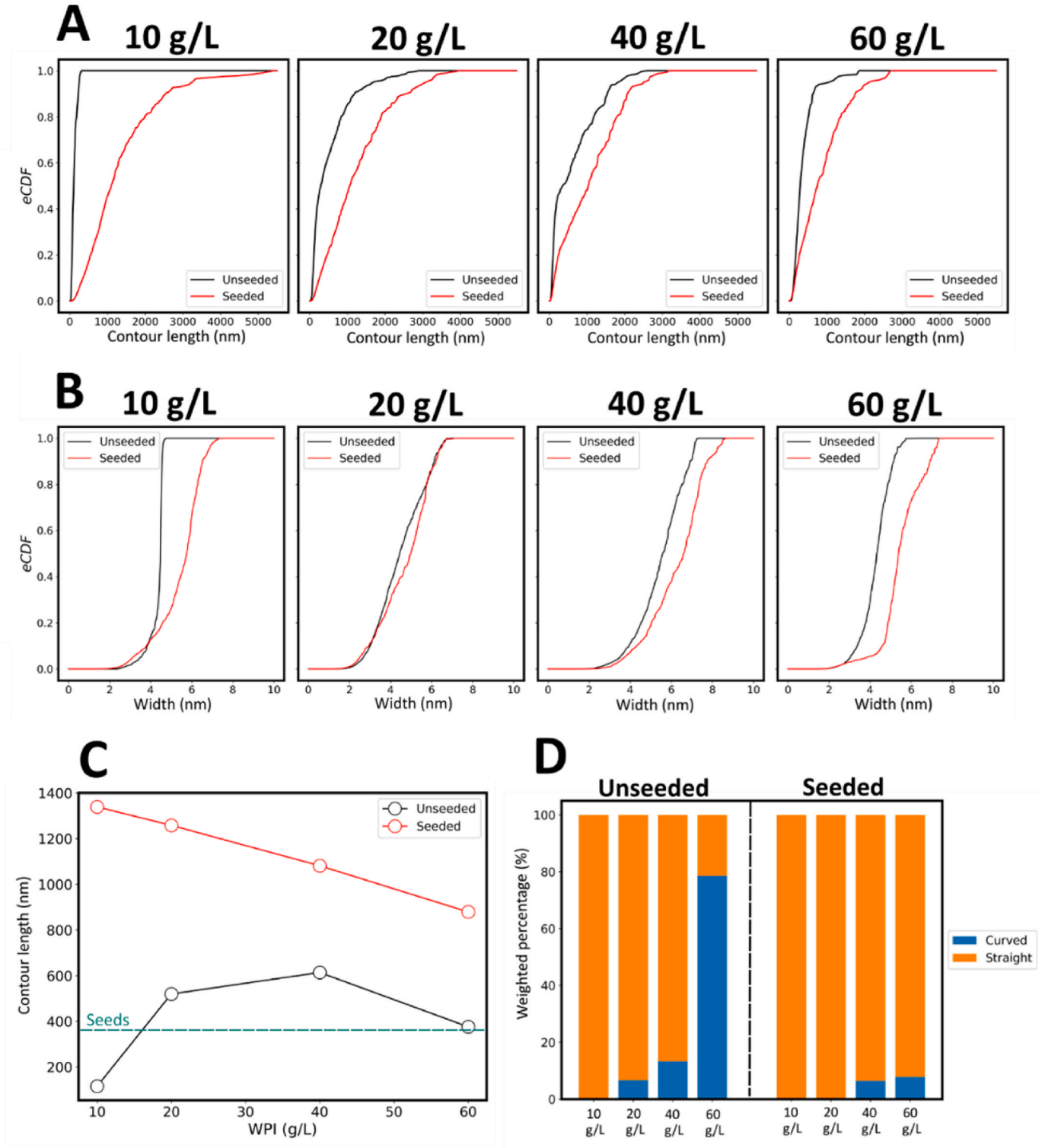

Fig. 4. (**A**) Weighted empirical cumulative distribution function (eCDF) of the fibril contour lengths of samples formed at pH 1.5 and the indicated WPI concentrations in the presence and absence of 10 % seeds and (**B**) the corresponding fibril width eCDFs. (**C**) The respective weighted average fibril contour length (L_c) as function of initial WPI concentration. The dashed green line represents the weighted average contour length of the seeds. (**D**) Weighted percentage of the amount of curved and straight PNFs in each of the samples depicted in panels A and B based on their persistence lengths. All samples were taken at their sol-gel transition as depicted in Fig. 1. (For interpretation of the references to color in this figure legend, the reader is referred to the Web version of this article.)

fibrillation reactions when seeds are added, emphasized by the fact that none of the ThT curves of seeded samples have any lag phase (Fig. 3A). Such is a stark contrast to the ThT curves of unseeded WPI, which have lag phases, especially at the lower WPI concentrations (Fig. 3B). The faster kinetics of the seeded samples are confirmed by extracting the reaction half-time ($t_{1/2}$) for each fibrillation curve. The double-logarithmic plots of $t_{1/2}$ against the initial protein concentration show that $t_{1/2}$ is much shorter for all seeded fibrillation reactions compared to reactions when seeds are absent (Fig. 3C).

For the lowest WPI concentrations (10 and 20 g/L), the observed sol-gel transition times seem to coincide with the very end of the induction phase (Fig. 3A), after which almost no difference in ThT signal is registered, while the gelation occurs during the exponential phase for the higher WPI concentrations. Notably, the ThT intensity of the samples is not directly related to the gel formation as some of the unseeded samples (that do not form gels) have higher final ThT intensities than some of the seeded samples (that do form gels). Hence, the amount (mass concentration) of PNFs is not the only determinant for if a sol-gel transition occurs.

3.5. Seed effect on fibril length and morphology

Since the gel formation in the seeded samples is not directly related to the mass concentration of PNFs, we moved on to investigate if the sol-gel transition could be due to changes in fibril length and morphology. For this purpose, we quantitatively characterized the single-fibril properties using AFM micrographs analyzed with FiberApp (Usov et al., 2015). Representative AFM images of the different samples and the employed seeds are shown in the Supplementary Material Figs. S1 and S2. We analyze PNF length distributions in the samples employing mass-weighted average values (in opposition to number averages) as this accounts for the fact that long fibrils contain significantly more protein building blocks than short fibrils. This is also the correct way to assess percolation due to the size polydispersity of PNFs, as demonstrated for percolation in carbon nanotube samples (Kyrylyuk & van der Schoot, 2008; Otten & van der Schoot, 2009). We then calculate the weighted empirical cumulative distribution function (eCDF). The approach is demonstrated by comparing the fibril contour length distributions of the seeds and the corresponding seeded samples after incubation (Fig. S3). The figure shows that after incubation, the eCDF curves are shifted towards longer contour lengths. Hence, the seeds elongate and become longer fibrils.

To investigate the gel formation, we analyzed the seeded samples by removing them from incubation at their sol-gel transition time (see Fig. 1D–F) and compared their length distributions to their respective unseeded counterparts at the *same time* as the sol-gel transition. The contour length eCDFs are shown in Fig. 4A and the distributions of fibril widths for the same samples are shown in Fig. 4B. The structural data is also summarized in Table S1. In all cases, samples fibrillated in the presence of seeds form substantially longer and slightly thicker PNFs than in the unseeded samples. This finding differs from previous results on WPI fibrillation reported by Bolder and co-workers (Bolder et al., 2007). In their experiments, seeding neither affected the fibrillation rate nor the length distribution of the fibrils. An explanation for this discrepancy may be that their experiments were carried out with vigorous stirring while our samples were incubated under quiescent conditions. Stirring can enhance the fragmentation of the fibrils and thereby have a similar effect as the addition of seeds. Hence, under the conditions used by Bolder et al. the addition of seeds may only lead to minor changes in the amount and length of the fibrils.

The change towards longer fibrils is made more obvious by plotting the weighted average contour length (L_c) for all samples (Fig. 4C, we here use uppercase letters to refer to population averages, while lowercase letters represent values for individual fibrils). Notably, we find a linear decrease in L_c in seeded samples with increasing WPI concentration. Such observation is indeed expected and is in line with the notion that, at higher concentrations, kinetic arrest and a percolation path can be achieved by shorter fibrils. For the non-seeded samples, we find an increase in L_c with increasing WPI concentrations in the range of 10–40 g/L, but then the trend changes and the 60 g/L sample has a lower average contour length. This is related to the previously reported morphology shift leading to the formation of curved PNFs at higher concentrations (Ye et al., 2018).

The clear decrease in fibrillation half-time in the presence of seeds (Fig. 3C), together with the observed formation of longer fibrils, shows that elongation must be the main molecular pathway for forming new fibrils in seeded reactions and the reason behind the sol-gel transition. If secondary nucleation, facilitated by the introduction of seeds, was the dominant process, a higher number of monomers would be allocated towards the formation of new secondary nuclei rather than elongating fibrils, hence resulting in a shorter but higher number of fibrils (Michaels et al., 2018). Given that fibrils in the presence of seeds are much longer than in unseeded WPI (especially evident for the 10 g/L sample, Fig. 4C), seed elongation must be the dominant aggregation process leading to gel formation. This observation makes sense, as primary nuclei are the aggregation species with the highest Gibbs free energy since nuclei growth by monomer addition needs to be faster than its dissociation into free monomers (Arosio et al., 2015; Buell et al., 2014; Michaels et al., 2018). Thus, it is understandable that monomer addition to seeds is less energetically demanding compared to the formation of new nuclei, even secondary nuclei. This conclusion also has important implications for interpreting the rise of a new population of straight PNFs at high (60 g/L) WPI concentration (Fig. 4D). As seed elongation is the dominant fibrillation process, the observed formation of straight PNFs in the presence of seeds is likely not the product of a curved-to-straight morphological conversion but rather a shift of the monomer mass allocation during aggregation towards the seed elongation pathway.

WPI can form straight and curved fibrils depending on the initial WPI concentration (Ye et al., 2018). The dominant presence of either morphology can dramatically impact material properties (Kamada et al., 2022; Kamada et al., 2017; Ye et al., 2022; Sanches Pires et al., 2025). To obtain a quantitative picture of the fibril morphology in each sample, we calculated the persistence length of individual PNFs (l_p) and classified them into two categories: straight ($l_p/l_c > 0.1$) and curved ($l_p/l_c \leq 0.1$), where l_c denotes the contour length of individual fibrils. We chose the value $l_p/l_c = 0.1$ to distinguish between curved/straight as this was the average l_p/l_c value registered for curved fibrils in the unseeded 60 g/L sample. In the unseeded solutions, curved PNFs are the dominant morphology at high (60 g/L) WPI concentration, while straight fibrils are dominant at concentrations equal to and below 40 g/L (Fig. 4D). Interestingly, there is a distinct switch in morphology from curved to straight PNFs when seeds are added at the high WPI concentration, as briefly reported in our previous work (Ye et al., 2018). The systematic investigation presented here shows that seeding has a pronounced effect in reducing the number of curved fibrils in all WPI concentrations, with special emphasis in the 60 g/L WPI sample, where the absence of seeding generates almost exclusively curved fibrils. This effect is likely related to the capture of newly formed monomers by the seeds (which have the straight morphology), which keeps them away from the alternative aggregation pathways that result in curved fibrils.

Taken together, we have shown that straight fibrils are the dominant morphology in seeded WPI and that seeding promotes the formation of significantly longer straight PNFs in comparison with unseeded WPI. As only seeded WPI experiences gelation, we can conclude that long straight fibrils are essential for the gelation process. In opposition, unseeded counterparts have much shorter PNFs with less prevalence of the straight morphology.

3.6. Hydrogel microstructure

As we have now clarified the relationship between the PNF morphology and the gel formation, the next step is to explore the fibrillar nature of the gels and the forces that characterize the formation and stabilization of their networks. For this, we focused on the gels formed from 20 g/L WPI at pH 1.5, as this sample forms exclusively straight PNFs, which is the dominant morphology in all studied gel samples. To access the architecture of the percolated fibrillar networks, we conducted SEM imaging of supercritically dried gel specimens. We see that the filamentous structures are organized into a highly porous network comprised of entangled filamentous structures (Fig. 5A and B). These arrangements seem globally isotropic in nature. At higher magnification (Fig. 5C and D), more detailed information about the local configuration of the percolating network can be inferred. At sol-gel transition time, this sample shows a weighted average height for single PNFs of about 4.7 ± 0.3 nm (Fig. 4B–Table S1), which is in good agreement with the diameter of the smallest filamentous structures seen in the SEM images (Fig. 5C and D). Most cell walls, however, appear to be thicker than single PNFs. The thickness of the fibrous structures measured in Fig. 5D is consistent with the hypothesis that single PNFs associate into higher-order filaments (Fig. 5E) via orientational ordering.

Additionally, the pore size distribution and structure seem to be relatively homogeneous throughout the sample surface, with pore diameters up to 100 nm (Fig. 5B and C). The AFM analysis of the redispersed sample shows a weighted average contour length for fibrils of 1.3 μm (Fig. 4C–Table S1), much larger than the apparent pore size measured in the SEM images. This means that one single PNF can participate in the build-up of several pore cell walls, thus intuiting the formation of a highly interlocked fibrillar network (see illustration in Fig. 5F). Altogether, the filamentous structures (pore cell walls) seem to comprise single PNFs and assemblies of several fibrils, indicating a locally anisotropic arrangement within a globally isotropic network (Kyrylyuk et al., 2008). This observation is complemented by the fact that, when this sample is observed between cross-polarizers, nematic droplets can be seen in the solution prior to gelation, which seem to disappear once a gel is formed (Fig. S4). Such behavior is not unusual, as colloidal suspensions of rod-like particles with a high aspect ratio in the isotropic phase can undergo both orientational ordering (Onsager, 1949) and kinetic arrest (Philipse, 1996) at similar volume fractions. For instance, the formation of gel networks from bundles of rods kinetically arrested in random orientations is a phenomenon that can be understood in the assembly of carbon nanotubes (Kyrylyuk et al., 2008).

3.7. Mechanical properties of the hydrogel

To understand the nature of the fibril-fibril interactions within the gel network, we performed rheological measurements on gels prepared at the same condition as depicted in SEM (20 g/L, 24 h incubation). Strain sweeps were used to record the gel's linear viscoelastic region (LVR) (Fig. 6A). After the determination of the LVR, a frequency sweep under a constant strain (0.1 % strain) was performed to obtain information about the linear viscoelastic response of the same gel condition (Fig. 6B). The pattern for the strain dependencies of the viscoelastic moduli shows a well-developed network, with the storage modulus, G', displaying a higher magnitude than the loss modulus, G'', i.e. $G' > G''$. A slight increase of G' with increasing angular frequency, ω, is also noted, which is a typical behavior demonstrated by weak physical gels (Matricardi et al., 2016). Useful information about the gel microstructure can also be obtained by looking into the large amplitude oscillatory shear (LAOS) region in a strain sweep, which refers to the moduli values within the non-linear viscoelastic region (defined by the region in which G' has experienced a decrease of more than 5 % compared to the value in

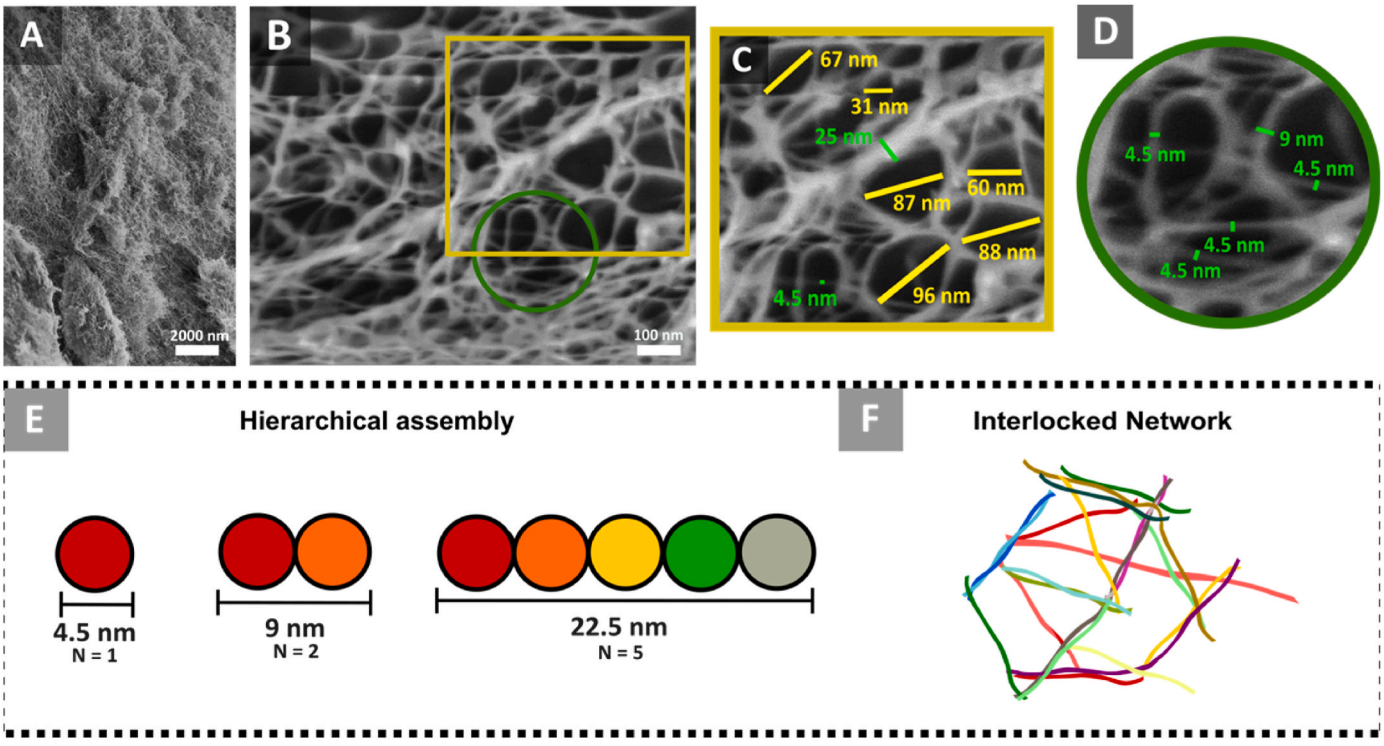

Fig. 5. (**A-D**) SEM images of a hydrogel specimen (20 g/L, 24 h incubation time) prepared via supercritical drying. The **A** and **B** panels relate to different magnifications and panels **C** and **D** correspond to two specific areas in Panel **B** as indicated by their colors. White thick lines represent scale bars. Yellow bars represent the diameter of pores, whereas green bars represent filament thickness. (**E, F**) Schematic representation of possible PNF association into higher hierarchical filaments comprised of N fibrils (**E**) and of the interlocked gel network (**F**). (For interpretation of the references to color in this figure legend, the reader is referred to the Web version of this article.)

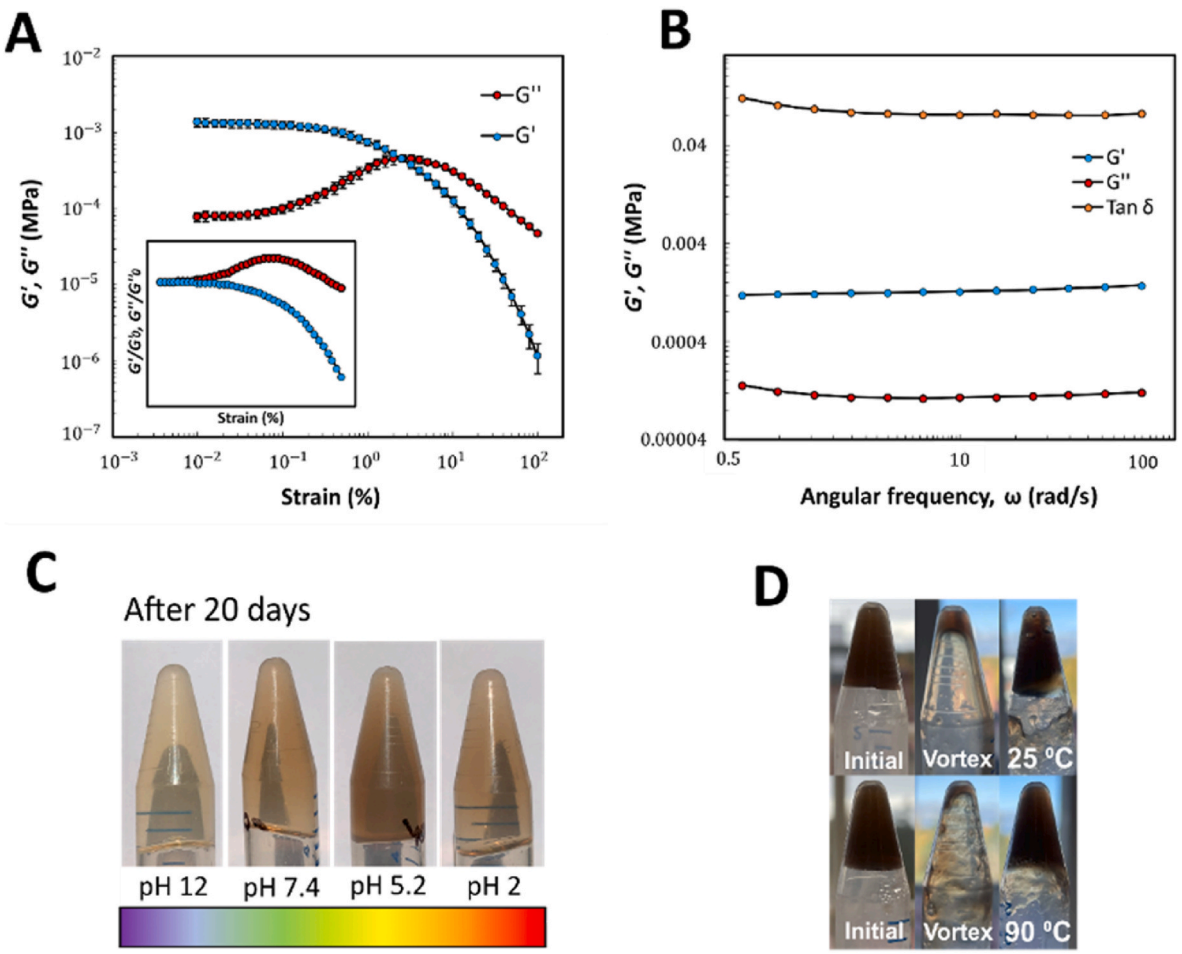

Fig. 6. (**A**) Strain sweep of a gel prepared at the same conditions as the one depicted in the SEM images in Fig. 5. The LVR was determined as the interval until a drop of less than 5 % from the initial value of G'. The inset depicts the reduced moduli G'/G_0' and G''/G''_0 over strain, where G'_0 and G''_0 are the moduli in the LVR. (**B**) Frequency sweep of the same gel at 0.1 % strain. Tan δ (i.e. G''/G') is also depicted. (**C**) Photographs of gels with solvent exchanged to solutions of different pH values and then incubated with those solutions for 20 days. (**D**) Seeded gels after vortexing and incubation at 25 °C or 90 °C.

the LVR). The behavior in the LAOS region is very sensitive to the interactions of microstructures within gel networks. At least four types of LAOS behavior have been described depending on the interaction between the different building blocks (Hyun et al., 2002). As can be seen in Fig. 6A, the pattern for the strain dependencies of the viscoelastic moduli displays a weak strain overshoot LAOS behaviour, similar to those of TEMPO-oxidized cellulose nanofibril hydrogels, multiwalled carbon nanotubes in water-oil emulsions, carbon black gels and hyaluronic acid fillers (Bhagavathi Kandy et al., 2018; Fan et al., 2019; Mendoza et al., 2018; Öhrlund, 2018). Here, the storage modulus G' decreases smoothly while the loss modulus G'' peaks and then decreases in an overshoot phenomenon. In many systems, this weak overshoot behavior is due to the breakage and recovery of weak physical bonds linking adjacent gel building blocks (Hyun et al., 2002; Matricardi et al., 2016). Considering the high stiffness of single PNFs (Knowles et al., 2007), it is unlikely that the decrease in G' and network dissociation following critical yield is due to the breakage of the fibrils themselves. As PNFs seem to assemble into bundled structures to form the pore walls, it is most likely that network disruption at critical strain occurs due to sliding and breakage of fibril-fibril interactions at the interface between different PNFs.

To further understand the intrinsic properties of the percolating network, we exposed gel specimens to solutions with different pH (between 2 and 12) for 20 days at 25 °C (Fig. 6C). As the aqueous phase of the gel is exchanged for a solution with higher pH, the intrinsic charge of the PNFs and the size of their surrounding electrical double-layer will be altered. If the inter-PNF interactions (as the ones generating the weak strain overshoot) were electrostatic in nature, changing both the electrical double layer and the fibril charge could promote gel instability and dissociation. Notably, we see that there is no apparent gel dissociation after 20 days of incubation at different pH, suggesting that the forces leading to gel formation and stabilization are not primarily electrostatic in nature. However, there may be minor changes in the gel properties, as made evident by the different coloration acquired by the gel incubated at pH 12 and the turbid aspect of the gel incubated with a solution of pH 5.2, which is close to the isoelectric point of β-lactoglobulin.

To understand the effect of high temperature in forming a percolating path, we destroyed the gel network by applying intensive shear via vortexing. Notably, the re-dispersed solutions can re-aggregate into a gel both when incubated at 25 °C and at 90 °C, showing the ability of the disrupted fibril-fibril interactions to recover and re-organize into a network, i.e., a self-healing behavior (Fig. 6D). Such observation also shows that the formation of a percolation path in the presence of fibrils is independent of high temperature and is, as expected for rod-like particles with a high aspect ratio, an inherent property of PNFs. However, high temperature is still essential for gelation as protein hydrolysis and fibril assembly are promoted by elevated temperature. Regardless, the fact that a gel can reform after disruption at 25 °C is a highly attractive property in areas such as the cosmetic industry (i.e. in the form of a cream, where "destruction" of the matrix due to skin application is following by re-structuration into a film).

3.8. Percolation of seed-elongated fibrils

Based on the detailed picture of the fibril properties derived from AFM in the studied samples (see section 3.5), we can consider the gelation process using percolation theory. The rheology and SEM data suggest the formation of a gel network comprised of both single and bundles of fibrils, which seem to be preceded by nematic droplet formation (Fig. S4). To simplify the interpretation of our data, we rationalized the percolation in our seeded systems under the light of connectedness percolation theory by treating sol-gel transition in the isotropic phase. In this case, we do not consider any adhesion forces in the definition of the percolation threshold and only consider kinetic arrest with the inclusion of the interfibrillar electrostatic repulsion. For suspensions of rod-like particles interacting via hard-core repulsion (impenetrable rods, see supplementary material), connectedness percolation theory gives the volume fraction at which geometric percolation occurs (Φ_p) as a function of the rod aspect ratio ($\gamma = L/D$) and the connectivity parameter (α) (details explained in the supporting information) (Schilling et al., 2015). For semi-flexible particles in the limit $L_c \approx L_p$, L_p becomes the relevant length scale (Odjik, 1977; Odjik, 1986; Odjik & Houwaart 1978). However, in most of our samples, the fibrils are in the hard-rod limit, $L_c < L_p$ (Table S1) and we therefore use L_c in our calculation of the percolation threshold. The only exception is the 60 g/L unseeded sample, for which L_p must be used as it contains mostly short, curved PNFs (see Table S1).

We also need to consider the soft electrostatic repulsion and double-layer effects originating from the charge properties of PNFs. Assuming a fully impenetrable double-layer simplifies this introduction. Thus, D_{eff} instead of D, becomes the physical limit for the hard-core interaction and α_{eff} the connectivity parameter (see details in the supporting information). For calculating the geometric features, charge properties and percolation thresholds, we consider the weighted average diameter from the AFM analysis of each sample (Table S1). A more challenging question when applying connectedness percolation theory is the value of the connectivity parameter. We estimate this value based on the predictions from the random contact model of packings of hard rods (Philipse, 1996; Philipse & Verberkmoes, 1997; Wouterse et al., 2009) and achieve a value of α_{eff} between 2.1 and 2.2 (see supporting information). We then considered this interval of connectedness to predict a range for the percolation thresholds for the gelling samples (Table 1 and Table S1). The calculated values show that the concentration thresholds for kinetic arrest in seeded samples are much lower than for the unseeded samples. This is expected since the PNFs in unseeded samples are much shorter (Fig. 4).

To compare the theoretical predictions for the percolation threshold and link the fibril dimensions and gelation, we determined the concentration of fibrils in our analyzed samples by removing the unfibrillated material via dialysis. The resulting fibril mass concentrations are listed in Table 1. At the lowest seeded WPI concentrations (10–20 g/L), the measured PNF concentrations at sol-gel transition are slightly lower than those predicted by the theory, given their dimensions and electrostatic properties (Table S1). On the other hand, the 40 and 60 g/L seeded samples seem to have a PNF concentration at sol-gel transition very close to what is predicted by the theory (Table 1). We interpret these results as a consequence of the rich phase-behaviour PNFs in solution and the impact of having the different ratios of fibril morphologies (curved vs. straight) present in each sample. For instance, the 10 and 20 g/L samples have a lower fibrillar mass at kinetic arrest than the one predicted by the theory. This discrepancy is likely due to several reasons. The first relates to the rod-like interpretation of PNFs, as we here use percolation theory applicable to hard (impenetrable) rods. Modelling PNFs and the resulting percolation based on soft-core (penetrable) rods (Mutiso et al., 2012) may be more adequate. A second issue is the degree of penetrability of the electrical double-layer. One could consider a certain degree of penetrability of the double layer, in which case γ_{eff} would acquire lower values than the ones presented in Table 1, thus lowering Φ_p. A last, yet relevant, possibility is related to attractive inter-PNF and unfavourable fibril-solvent hydrophobic interactions. Given the rheology data presented in the previous section, adhesion forces could play an important role in the sol-gel transition. Any form or magnitude of short-ranged attractive potential between fibrils would drastically lower the percolation threshold (Kyrylyuk & van der Schoot, 2008), which could explain the lower fibrillar mass at the sol-gel transition we found compared to the theory.

To explain the agreement between fibrillar mass concentration at kinetic arrest and their predicted percolation for the higher WPI concentrations (Table 1), we would like to draw attention to the fact that 10–20 g/L seeded WPI form exclusively straight PNFs at sol-gel transition while the higher concentrations (40 g/L and 60 g/L) contains a small portion of curved PNFs (Fig. 4D). One conclusion could be that the curved fibrils do not contribute to percolation, meaning that these samples have a lower efficient (straight) PNF concentration than that measured here. Bending flexibility affects the percolation threshold, which is especially true for very flexible polymers such as curved PNFs, with axes that may fold back onto themselves (Otten & van der Schoot, 2009). The treatment of curved PNFs as hard rods results in an underestimation of the concentration requirements for kinetic arrest in these samples. Hence, qualitative and quantitative agreement of the theory and experiments at higher WPI concentrations is likely due to an underestimation of the Φ_p due to the presence of curved PNFs. Regardless, with these sources of error in mind, the predicted values are indeed in reasonably good agreement with the experimental results.

Table 1
Experimentally measured fibril concentration at sol-gel transition for each sample compared to their respective predicted percolation threshold according to the properties summarized in Table S1 of unseeded and seeded WPI. The unseeded samples for each WPI concentration (which do not gel) were collected at the same time as their seeded counterparts form a gel.

Sample		Measured fibril mass (g/L)	Predicted percolation (g/L)
10 g/L	No seed	0.8 ± 0.3	128–232
	Seeded	4.7 ± 0.6	19–38
20 g/L	No seed	3.7 ± 0.1	47–91
	Seeded	10.8 ± 0.6	22–43
40 g/L	No seed	24.7 ± 0.3	48–92
	Seeded	27.7 ± 0.2	30–58
60 g/L	No seed	36.2 ± 0.4	103–191
	Seeded	41.1 ± 1.8	33–69

4. Conclusions

We have in this work elucidated the fundamental mechanisms underlying the gelation of WPI induced by the addition of PNF seeds. We found that the gels are formed by a network of nanofibrils and that percolation in seeded WPI is achieved due to an amplification of the fibril elongation processes provided by the seeds. This process drastically speeds up fibrillation and enhances the formation of substantially longer fibrils compared to unseeded WPI. It also provides a shift in fibril morphology from shorter, curved fibrils to longer, straight ones. The morphological transition facilitated by seeds, including the formation of longer fibrils, is critical as it lowers the percolation threshold, allowing gelation at lower fibrillar mass concentrations (as low as 4 g/L WPI, Table 1). Our findings also highlight the relation between protein hydrolysis and the rate of fibril formation and, thereby, the gelation time as well as the amount of fibrillar material formed. The results suggest that the seeds effectively catalyze the allocation of hydrolyzed peptides into the fibril elongation pathway.

The rheological analysis demonstrates the physical nature of the gels, revealing a robust network stabilized predominantly by interactions that are not of electrostatic nature, as evidenced by the stability of the gel network across a wide pH range. Moreover, the application of continuum percolation theory provided a theoretical framework that

corroborates the experimental observations. This study advances our understanding of the sol-gel transition in fibrillar protein systems and underscores the potential of seeded gelation as a technique for tuning the mechanical and structural properties of protein-based materials. By manipulating seeding and pH, it is possible to design protein hydrogels with specific textures and functionalities for diverse applications in food technology, materials science, and biomedicine.

CRediT authorship contribution statement

Rodrigo Sanches Pires: Writing – original draft, Visualization, Methodology, Investigation, Formal analysis, Conceptualization. **Antonio J. Capezza:** Writing – review & editing, Investigation, Formal analysis. **Mathias Johansson:** Writing – review & editing, Investigation, Formal analysis. **Maud Langton:** Writing – review & editing, Supervision, Resources. **Christofer Lendel:** Writing – review & editing, Supervision, Project administration, Funding acquisition, Conceptualization.

Declaration of competing interest

The authors declare that they have no known competing financial interests or personal relationships that could have appeared to influence the work reported in this paper.

Acknowledgment

We thank Rasmus Mörtberg for the experimental pre-study and Eric Tyrode for help with polarized light microscopy. ÅForsk (grant nr 22-63) and the Swedish Research Council (grant nr 2020-03329) are acknowledged for financial support.

Appendix A. Supplementary data

Supplementary data to this article can be found online at https://doi.org/10.1016/j.foodhyd.2025.111424.

Data availability

Data will be made available on request.

References

Akkermans, C., Venema, P., van der Goot, A. J., Gruppen, H., Bakx, E. J., Boom, R. M., et al. (2008). Peptides are building blocks of heat-induced fibrillar protein aggregates of β-lactoglobulin formed at pH 2. *Biomacromolecules, 9*, 1474–1479.
Arosio, P., Knowles, T. P., & Linse, S. (2015). On the lag phase in amyloid fibril formation. *Physical Chemistry Chemical Physics, 17*, 7606–7618.
Bateman, L., Ye, A., & Singh, H. (2010). In vitro digestion of β-lactoglobulin fibrils formed by heat treatment at low pH. *Journal of Agricultural and Food Chemistry, 58*, 9800–9808.
Bhagavathi Kandy, S., Simon, G. P., Cheng, W., Zank, J., Joshi, K., Gala, D., et al. (2018). Effect of incorporation of multiwalled carbon nanotubes on the microstructure and flow behavior of highly concentrated emulsions. *ACS Omega, 3*, 13584–13597.
Boissonade, J., Barreau, F., & Carmona, F. (1983). The percolation of fibres with random orientations: A Monte Carlo study. *Journal of Physics A: Mathematical and General, 16*, 2777–2787.
Bolder, S. G., Hendrickx, H., Sagis, L. M., & van der Linden, E. (2006). Fibril assemblies in aqueous whey protein mixtures. *Journal of Agricultural and Food Chemistry, 54*, 4229–4234.
Bolder, S. G., Sagis, L. M. C., Venema, P., & van der Linden, E. (2007). Effect of stirring and seeding on whey protein fibril formation. *Journal of Agricultural and Food Chemistry, 55*, 5661–5669.
Buell, A. K. (2019). The growth of amyloid fibrils: Rates and mechanisms. *Biochemical Journal, 476*, 2677–2703.
Buell, A. K., Dobson, C. M., & Knowles, T. P. (2014). The physical chemistry of the amyloid phenomenon: Thermodynamics and kinetics of filamentous protein aggregation. *Essays in Biochemistry, 56*, 11–39.
Cao, Y., & Mezzenga, R. (2020). Design principles of food gels. *Nature Food, 1*, 106–118.
Chiti, F., & Dobson, C. M. (2006). Protein misfolding, functional amyloid, and human disease. *Annual Review of Biochemistry, 75*, 333–366.
Cohen, S. I. A., Linse, S., Luheshi, L. M., Hellstrand, E., White, D. A., Rajah, L., et al. (2013). Proliferation of amyloid-β42 aggregates occurs through a secondary nucleation mechanism. *Proceedings of the National Academy of Sciences U. S. A., 110*, 9758–9763.
Dave, A. C., Loveday, S. M., Anema, S. G., Loo, T. S., Norris, G. E., Jameson, G. B., et al. (2013). Beta-lactoglobulin self-assembly: Structural changes in early stages and disulfide bonding in fibrils. *Journal of Agricultural and Food Chemistry, 61*, 7817–7828.
Fan, X., Xu, H., Zhang, Q., Xiao, D.e., Song, Y., & Zheng, Q. (2019). Insight into the weak strain overshoot of carbon black filled natural rubber. *Polymer, 167*, 109–117.
Gade Malmos, K., Blancas-Mejia, L. M., Weber, B., Buchner, J., Ramirez-Alvarado, M., Naiki, H., et al. (2017). ThT 101: A primer on the use of thioflavin T to investigate amyloid formation. *Amyloid: International Journal of Experimental & Clinical Investigation, 24*, 1–16.
Gosal, W. S., Clark, A. H., & Ross-Murphy, S. B. (2004). Fibrillar β-lactoglobulin gels: Part 1. Fibril formation and structure. *Biomacromolecules, 5*, 2408–2419.
Hoppenreijs, L. J. G., Fitzner, L., Ruhmlieb, T., Heyn, T. R., Schild, K., van der Goot, A. J., et al. (2022). Engineering amyloid and amyloid-like morphologies of β-lactoglobulin. *Food Hydrocolloids, 124*, Article 107301.
Housmans, J. A. J., Houben, B., Monge-Morera, M., Asvestas, D., Nguyen, H. H., Tsaka, G., et al. (2022). Investigating the sequence determinants of the curling of amyloid fibrils using ovalbumin as a case study. *Biomacromolecules, 23*, 3779–3797.
Hyun, K., Kim, S. H., Ahn, K. H., & Lee, S. J. (2002). Large amplitude oscillatory shear as a way to classify the complex fluids. *Journal of Non-newtonian Fluid Mechanics, 107*, 51–65.
Jarrett, J. T., & Lansbury, P. T., Jr. (1993). Seeding "one-dimensional crystallization" of amyloid: A pathogenic mechanism in Alzheimer's disease and scrapie? *Cell, 73*, 1055–1058.
Kamada, A., Herneke, A., Lopez-Sanchez, P., Harder, C., Ornithopoulou, E., Wu, Q., et al. (2022). Hierarchical propagation of structural features in protein nanomaterials. *Nanoscale, 14*, 2502–2510.
Kamada, A., Mittal, N., Söderberg, L. D., Ingverud, T., Ohm, W., Roth, S. V., et al. (2017). Flow-assisted assembly of nanostructured protein microfibers. *Proceedings of the National Academy of Sciences USA, 114*, 1232–1237.
Kavanagh, G. M., Clark, A. H., & Ross-Murphy, S. B. (2000). Heat-induced gelation of globular proteins: 4. Gelation kinetics of low pH β-lactoglobulin gels. *Langmuir, 16*, 9584–9594.
Knowles, T. P., Fitzpatrick, A. W., Meehan, S., Mott, H. R., Vendruscolo, M., Dobson, C. M., et al. (2007). Role of intermolecular forces in defining material properties of protein nanofibrils. *Science, 318*, 1900–1903.
Kyrylyuk, A. V., & van der Schoot, P. (2008). Continuum percolation of carbon nanotubes in polymeric and colloidal media. *Proceedings of the National Academy of Sciences USA, 105*, 8221–8226.
Langton, M., & Hermansson, A.-M. (1992). Fine-stranded and particulate gels of β-lactoglobulin and whey protein at varying pH. *Food Hydrocolloids, 5*, 523–539.
Lendel, C., & Solin, N. (2021). Protein nanofibrils and their use as building blocks of sustainable materials. *RSC Advances, 11*, 39188–39215.
Linse, S. (2017). Monomer-dependent secondary nucleation in amyloid formation. *Biophysical Reviews, 9*, 329–338.
Loveday, S. M., Anema, S. G., & Singh, H. (2017). β-Lactoglobulin nanofibrils: The long and the short of it. *International Dairy Journal, 67*, 35–45.
Matricardi, P., Alhaique, F., & Coviello, T. (2016). *Polysaccharide hydrogels: Characterization and biomedical applications*. Pan Stanford Publishing.
Meisl, G., Kirkegaard, J. B., Arosio, P., Michaels, T. C., Vendruscolo, M., Dobson, C. M., et al. (2016). Molecular mechanisms of protein aggregation from global fitting of kinetic models. *Nature Protocols, 11*, 252–272.
Mendoza, L., Batchelor, W., Tabor, R. F., & Garnier, G. (2018). Gelation mechanism of cellulose nanofibre gels: A colloids and interfacial perspective. *Journal of Colloid and Interface Science, 509*, 39–46.
Michaels, T. C. T., Saric, A., Habchi, J., Chia, S., Meisl, G., Vendruscolo, M., et al. (2018). Chemical kinetics for bridging molecular mechanisms and macroscopic measurements of amyloid fibril formation. *Annual Review of Physical Chemistry, 69*, 273–298.
Mutiso, R. M., Sherrott, M. C., Li, J., & Winey, K. I. (2012). Simulations and generalized model of the effect of filler size dispersity on electrical percolation in rod networks. *Physical Review B, 86*, Article 214306.
O'Nuallain, B., Williams, A. D., Westermark, P., & Wetzel, R. (2004). Seeding specificity in amyloid growth induced by heterologous fibrils. *Journal of Biological Chemistry, 279*, 17490–17499.
Odijk, T. (1977). Polyelectrolytes near the rod limit. *Journal of Polymer Science Polymer Physics Edition, 15*, 477–483.
Odijk, T. (1986). Theory of lyotropic polymer liquid crystals. *Macromolecules, 19*, 2313–2329.
Odijk, T., & Houwaart, A. C. (1978). On the theory of the excluded-volume effect of a polyelectrolyte in a 1-1 electrolyte solution. *Journal of Polymer Science Polymer Physics Edition, 16*, 627–639.
Öhrlund, Å. (2018). Evaluation of rheometry amplitude sweep cross-over point as an index of flexibility for HA fillers. *Journal of Cosmetics, Dermatological Sciences and Applications, 8*, 47–54.
Onsager, L. (1949). The effects of shape on the interaction of colloidal particles. *Annals of the New York Academy of Sciences, 51*, 627–659.
Otten, R. H. J., & van der Schoot, P. (2009). Continuum percolation of polydisperse nanofillers. *Physical Review Letters, 103*, Article 225704.
Philipse, A. P. (1996). The random contact equation and its implications for (colloidal) rods in packings, suspensions, and anisotropic powders. *Langmuir, 12*, 1127–1133.
Philipse, A. P., & Verberkmoes, A. (1997). Statistical geometry of caging effects in random thin-rod structures. *Physica A: Statistical Mechanics and Its Applications, 235*, 186–193.

Puyol, P., Pérez, M. D., & Horne, D. S. (2001). Heat-induced gelation of whey protein isolates (WPI): Effect of NaCl and protein concentration. *Food Hydrocolloids, 15*, 233–237.

Rahman, M. M., Pires, R. S., Herneke, A., Gowda, V., Langton, M., Biverstål, H., et al. (2023). Food protein-derived amyloids do not accelerate amyloid beta aggregation. *Scientific Reports, 13*, 985.

Roode, L. W. Y., Shimanovich, U., Wu, S., Perrett, S., & Knowles, T. P. J. (2019). Protein microgels from amyloid fibril networks. In *Biological and bio-inspired nanomaterials. Advances in experimental medicine and biology* (Vol. 1174)Singapore: Springer.

Sanches Pires, R., Capezza, A. J., Jonsson, D., Lyrner Morén, J., Hedenqvist, M. S., & Lendel, C. (2025). Elucidating the role of the nanostructure in protein aerogels for removal of organic water pollutants. *RSC Sustainability, 2*, 4036–4045.

Scheidt, T., Lapinska, U., Kumita, J. R., Whiten, D. R., Klenerman, D., Wilson, M. R., et al. (2019). Secondary nucleation and elongation occur at different sites on Alzheimer's amyloid-beta aggregates. *Science Advances, 5*, Article eaau3112.

Schilling, T., Miller, M. A., & Van der Schoot, P. (2015). Percolation in suspensions of hard nanoparticles: From spheres to needles. *Europhysics Letters, 111*, Article 56004.

Shi, L., & Dee, D. R. (2024). Seeding and gelation properties of lentil protein nanofibrils. *Food Hydrocolloids, 156*, Article 110360.

Stading, M., & Hermansson, A.-M. (1990). Viscoelastic behaviour of β-lactoglobulin gel structures. *Food Hydrocolloids, 4*, 121–135.

Stading, M., & Hermansson, A.-M. (1991). Large deformation properties of β-lactoglobulin gel structures. *Food Hydrocolloids, 5*, 339–352.

Thacker, D., Barghouth, M., Bless, M., Zhang, E., & Linse, S. (2023). Direct observation of secondary nucleation along the fibril surface of the amyloid β 42 peptide. *Proceedings of the National Academy of Sciences USA, 120*, Article e2220664120.

Törnquist, M., Michaels, T. C. T., Sanagavarapu, K., Yang, X., Meisl, G., Cohen, S. I. A., et al. (2018). Secondary nucleation in amyloid formation. *Chem Commun (Camb), 54*, 8667–8684.

Uniacke-Lowe, T., & Fox, P. F. (2022). Equid milk. In *Encyclopedia of dairy sciences* (pp. 543–556).

Usov, I., & Mezzenga, R. (2015). FiberApp: An open-source software for tracking and analyzing polymers, filaments, biomacromolecules, and fibrous objects. *Macromolecules, 48*, 1269–1280.

vandenAkker, C. C., Engel, M. F., Velikov, K. P., Bonn, M., & Koenderink, G. H. (2011). Morphology and persistence length of amyloid fibrils are correlated to peptide molecular structure. *Journal of the American Chemical Society, 133*, 18030–18033.

Veerman, C., Ruis, H., Sagis, L. M., & van der Linden, E. (2002). Effect of electrostatic interactions on the percolation concentration of fibrillar β-lactoglobulin gels. *Biomacromolecules, 3*, 869–873.

Wouterse, A., Luding, S., & Philipse, A. P. (2009). On contact numbers in random rod packings. *Granular Matter, 11*, 169–177.

Xu, D., Zhou, J., Soon, W. L., Kutzli, I., Molière, A., Diedrich, S., et al. (2023). Food amyloid fibrils are safe nutrition ingredients based on in-vitro and in-vivo assessment. *Nature Communications, 14*, 6806.

Ye, X., Capezza, A. J., Davoodi, S., Wei, X.-F., Andersson, R. L., Chumakov, A., et al. (2022). Robust assembly of cross-linked protein nanofibrils into hierarchically structured microfibers. *ACS Nano, 16*, 12471–12479.

Ye, X., Hedenqvist, M. S., Langton, M., & Lendel, C. (2018). On the role of peptide hydrolysis for fibrillation kinetics and amyloid fibril morphology. *RSC Advances, 8*, 6915–6924.